Flowfield Vorticity Calculation using PIV Data

Lecuona, A.*, Nogueira, J. I.* and Rodríguez, P. A.*

* Universidad Carlos III de Madrid, Department of Mechanical Engineering, 28911-Leganés, Madrid, Spain.

Abstract: The simultaneous velocity measurement at different flowfield locations is one of the key advantages of a PIV system. This allows a straightforward calculation of derived flow magnitudes including spatial correlations. Thus, postprocessing techniques need further attention in order to assure maximum feature extraction with minimum error, among other issues. This paper is devoted to expand the capability of calculating vorticity in a PIV sampled flow field. The methodology proposed is based on linear algorithms (FIR filters) able to obtain the first spatial derivative of a grid sampled magnitude containing random noise. Generalization to other flow magnitudes based on spatial derivatives is immediate. Been this a widely used method, the main objective of the study is to develop new filters from families already documented. The relevant performance parameters of these filters are evaluated and commented. Synthetic data fields are used to test the basic metrological attributes in a controlled way. As a result of the study, algorithms with better performances than the usual ones are proposed and strong points are highlighted. Finally, results of the application to real PIV data are exhibited and commented.

Keywords: PIV, vorticity, spatial derivatives, FIR filters, adaptive filters.

1. Introduction

This work assumes that discrete information of a smooth magnitude a including additive random noise ε is given on the equally spaced points of a two dimensional grid (x, y). In a typical PIV system output a would be either of the velocity components. $\varepsilon(x, y)$ represents the acceptable errors, this means that it does not include erroneous vectors that are supposed to have been removed by validation algorithms, like the ones described by Raffel and Kompenhans (1996) or Nogueira et al. (1997). Our objective is to establish a method able to calculate the first spatial derivatives $(\partial/\partial x, \partial/\partial y)$, on the same grid points, with both as high as possible accuracy and noise rejection. The length unit used to calculate derivatives is the grid spacing, and the obtained magnitude will be called b. Where the ideal analytical derivatives (instead of the numerically calculated) are invoked, they will be called b^*.

The methods presented in this article carry out the following operation:

$$b_{0,0} = \frac{\sum_{i,j} a_{i,j}\, \eta_{i,j}}{\alpha} \; ; \; |i| \leq n \; ; \; |j| \leq m \tag{1}$$

Where α and $\eta_{i,j}$ are constants. $\eta_{i,j}/\alpha$ forms the filter impulse response. Figure 1 shows a pictorial view of this algorithm with $n = m$. When $n \neq m$, the key to identify each $\eta_{i,j}$ is that $\eta_{0,0}$ will be always in the centre.

$$\frac{1}{\alpha}$$

$\eta_{-2,-2}$	$\eta_{-1,-2}$	$\eta_{0,-2}$	$\eta_{1,-2}$	$\eta_{2,-2}$
$\eta_{-2,-1}$	$\eta_{-1,-1}$	$\eta_{0,-1}$	$\eta_{1,-1}$	$\eta_{2,-1}$
$\eta_{-2,0}$	$\eta_{-1,0}$	$\eta_{0,0}$	$\eta_{1,0}$	$\eta_{2,0}$
$\eta_{-2,1}$	$\eta_{-1,1}$	$\eta_{0,1}$	$\eta_{1,1}$	$\eta_{2,1}$
$\eta_{-2,2}$	$\eta_{-1,2}$	$\eta_{0,2}$	$\eta_{1,2}$	$\eta_{2,2}$

Fig. 1. Nomenclature for linear filters.

Initially, the derivation will be assumed along the x direction. Filters to calculate the derivative along the y direction are just a $90°$ rotation of the former ones. Vorticity is calculated just by addition: $\omega = \partial v_y / \partial x - \partial v_x / \partial y$
Other nomenclature used in this article is:

A: Amplitude of the Fourier component of a under study.
λ_x, λ_y :   Wavelengths of the Fourier component under study, measured in grid units along x and y directions respectively.
$\Delta x, \Delta y$: $2\pi/\lambda_x$ and $2\pi/\lambda_y$ respectively.
σ_ε :   Standard deviation of the data noise.
rms :   Root mean square.
rmse :   Root mean square error.

As much as 12 filters will be referenced along this work. Some of them ("a", "b", "d") are usual filters brought for performance reference. Some others ("c", "e", "f") just show the impossibility of obtaining clearly good results by following a certain design methodology. Finally, filters "i" and "j" are presented as an improvement in performance in relation to usual ones.

2. Errors on the Calculation of the First Derivative

Two factors affect the accuracy of operation (1): the discrete nature of the data and the presence of noise. To deal with them the following approach has been chosen:

- Each spatial Fourier component of a is analyzed separately. Due to the linearity of the filter, the response to the sum of components is the sum of responses.
- The noise in the data is modeled as an additive stochastic effect that reaches a certain percentage of the numeric data range. In this work it will be considered as a random variable, whose standard deviation is proportional to the amplitude of the Fourier component of a.

Based on these two considerations, analysis of each Fourier component is performed, modeled as: $a = A \cdot \sin(x2\pi/\lambda_x)\sin(y2\pi/\lambda_y)$, similarly as Agüi and Jiménez (1987). Additional noise, ε, is included so that data are formed by $a+\varepsilon$. The result of filtering this synthetic flow magnitude is then compared with its analytical derivation. This allows a consistent error evaluation. After some analytical work, Equation (2) arises for the resulting total error, when $b_{0,0}$ is predicted through Equation (1). The steps to obtain this result can be summarized as follows:

1. Substituting $a_{i,j}$ in Equation (1) by its Taylor expansion centered at $i,j = 0,0$.
2. Expressing the successive derivatives of a as function of $\partial a/\partial x|_{0,0}$ (remember that a is now a known Fourier component)
3. Reassembling the terms on Δx and Δy as if they were components of a Taylor expansion.

$$\frac{\text{rmse}}{\text{rms}(b*)} = \sqrt{\left[1 - \sum_{i,j} \frac{\eta_{i,j}}{\alpha \Delta x} \sin(i\Delta x)\cos(i\Delta j)\right]^2 + \left[\frac{2\sigma_\varepsilon}{A\alpha \Delta x} \sqrt{\sum_{i,j} \eta_{i,j}^2}\right]^2} \tag{2}$$

These steps are explained in more detail in Nogueira et al. (1997). Equation (2) gives an idea of the relative error in b for any linear derivating filter in a region where a certain Fourier component is dominant. It is also of value to show when the *rmse* grows to unbearable levels:

- When approaching the Nyquist wavelength, $\lambda_x \to 2$, this is equivalent to $\Delta x \to \pi$. Then the first term tends to 1 in any case. This effect is due to the discrete nature of the data. It is shown on the left part of Fig. 2. Symmetry in the impulse response coefficients implies that the response to the Nyquist frequency is null, leading to 100% error.
- At long wavelengths $\Delta x \to 0$ and consequently, the second term dominates as $1/\Delta x$. This effect is due to the presence of noise, and can not be eliminated by looking for a higher order filter. It is shown on the right part of Fig. 2. What can only be done is a vertical shift of the straight line representing $1/\Delta x$. This effect is somewhat misleading, because here the error is based on the amplitude of the single harmonic, not on its derivative which is proportional to Δx. Besides that, the experimenter is rarely interested on very long wavelengths, which imply very small values of the derivative, specially when dealing with vorticity. This magnitude normally is of interest when it is concentrated.

3. Design of Suitable First Derivative Filters

Some arbitrary, but judicious, restrictions have been added to limit the class of filters studied. In order to preserve phase this work focuses on antisymmetric filters about the y axis but symmetric about the x axis ($\Rightarrow 0 = \Sigma \eta_{i,j}$). The filters have to be at least first order accurate in respect to the derivative ($\Rightarrow \alpha = \Sigma i \eta_{i,j}$) The chosen noise for the synthetic field used for evaluation of the filters is an uncorrelated random value of a uniform probability density distribution of maximum amplitude 0.1A, thus compatible with Equation (2). This means that $\sigma_\varepsilon/A = 0.1/\sqrt{3}$. This is a representative level, typical of video based PIV systems, for relatively noisy images. Extension to either lower or higher noise levels is straightforward.

With these restrictions, an optimization process has been used to determine all the filter coefficients. The criterion for optimization is to minimize the integration of $(\text{rmse}/\text{rms}(b*))^2$, given by expression (2), between two wavelengths. One is representative of the shortest wavelengths, near Nyquist condition, and in the area where PIV statistical processing could still give reliable information by orthodox correlation peak fitting. It will be called λ_1. The other wavelength, λ_2, is representative of the longest wavelength that could be described with not such high error to make results useless, owing to the noise content. The weighting in the integration was selected to be logarithmic (this way the lap between a particular frequency and a certain multiple is always weighted the same). The rationale behind this otherwise arbitrary choice is that the shortest wavelengths should be weighted more as PIV is generally asked for describing these frequencies. Rarely the flow field is sampled so densely such that all its frequency content means large values for λ, specially with video recording and/or turbulent flows. The resulting equations are as follows:

$$\frac{\partial}{\partial \eta_{i,j}} \left[\int_{\lambda_{y1}}^{\lambda_{y2}} \left[\int_{\lambda_{x1}}^{\lambda_{x2}} \left(\frac{\text{rmse}}{\text{rms}(b*)}\right)^2 d(\ln(\lambda_x))\right] d(\ln(\lambda_y))\right] = 0 \tag{3}$$

This scheme produces what will be called from now on "optimized derivative filters".

In the following paragraphs some types of filters are compared using Equation (2).

3.1. Evaluation of One Dimensional Linear Filters

The first type of filters to be analyzed are one-dimensional examples ($\eta_{i,j} = 0 \; \forall \; j \neq 0$). Traditionally, first and second order schemes have been used to calculate the first derivative (respectively filters "a" and "b" in Fig. 2). To illustrate the use of Equation (3), filter "c" has been obtained minimizing the error in the range $\lambda_x \in (2.75, 22)$ and allowing for 13 coefficient filters. The resulting error is shown in Fig. 2.

FILTER:

(a)

$$\frac{1}{2} \quad \boxed{-1} \; \boxed{0} \; \boxed{1}$$

(b)

$$\frac{1}{12} \quad \boxed{1} \; \boxed{-8} \; \boxed{0} \; \boxed{8} \; \boxed{1}$$

(c)

$$\frac{1}{1200} \quad \boxed{32} \; \boxed{158} \; \boxed{-171} \; \boxed{107} \; \boxed{-31} \; \boxed{-803} \; \boxed{0} \; \boxed{803} \; \boxed{31} \; \boxed{-107} \; \boxed{171} \; \boxed{-158} \; \boxed{-32}$$

R.M.S.E. versus Wavelength (Signal=2sin(x2π/λx)sin(y2π/λy))
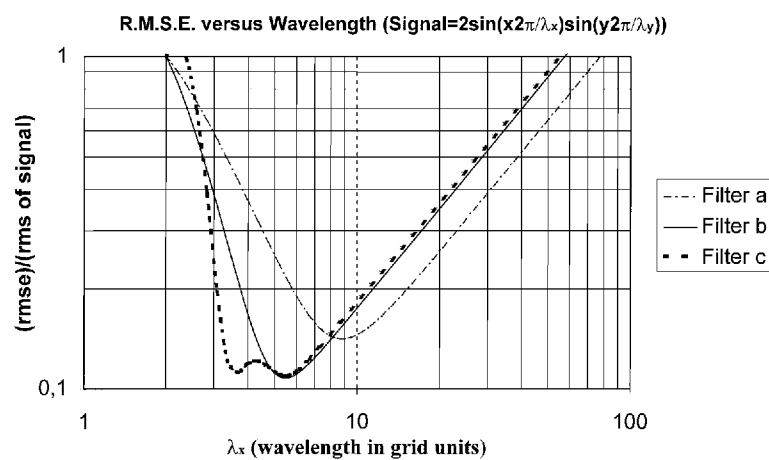
Fig. 2.   Total error of 1D derivating filters at different spatial frequencies.

The results given by filter "c" are not so impressive, although it shows lower error at short wavelengths. It can be argued that its behavior at long wavelengths is worse than that from filters "a" and "b". This comes from a higher value of $\Sigma\eta_{i,j}{}^2/\alpha$, which increases the random error amplification factor. Any other 1D filter with less coefficients would give inferior performance. If some improvement is forced at long wavelengths deterioration raises at short ones. And the reverse phenomenon happens for the inverse action. This shows that a reasonably long one-dimensional linear filter is not capable of performing satisfactorily over a broad wavelength interval.

3.2. Some Two-dimensional Filters

These filters introduce errors from the non linear variation of a along the traverse direction, y direction in this case, but bring the capability of further reducing noise in the data, owing to their higher averaging effect. More precisely, this is due to the possibility of reducing the value of $\Sigma\eta_{i,j}{}^2/\alpha$ as the number of coefficients increase, decreasing the second term inside the square root of Equation (2). Using Equation (3) a variety of two-dimensional filters can be designed. Reasonable filter size calls for a 5 by 5 matrix size to avoid too much information loss at the rim of the flowfield and to consume a reasonable computing time. Comparison with the usual "circulation method filter" (filter "d" in Fig. 3) is a valuable test as this filter has been recently proposed as a good candidate by Abrahamson and Lonnes (1995). The two filters shown as examples of the optimizing process were designed for λ_x ,$\lambda_y \in (2.5,$ 22) (filter "e" in Fig. 3) and λ_x ,$\lambda_y \in (5, 22)$ (filter "f" in Fig. 3). Their respective error surfaces are plotted in Figs. 4, 5 and 6 (note that on these pictures the axis are not logarithmic). As filter "e" has been optimized for shorter wavelengths than filter "d" its error is much more less in this respect, but unfortunately is larger at long wavelengths. Comparison of these results with the ones already obtained for the 1D filters is possible using Fig. 7, made for the particular case of $\lambda_x = \lambda_y$, which in turns makes it possible a direct comparison with those in Fig. 2.
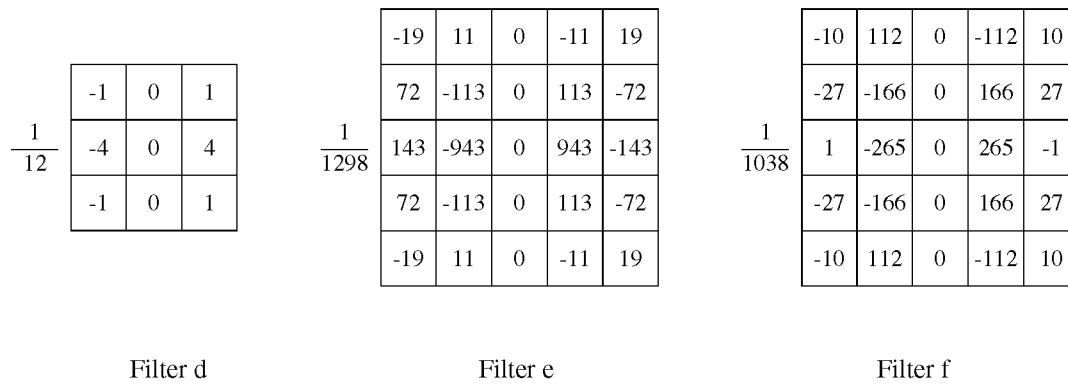
$$\frac{1}{12}$$

-1	0	1
-4	0	4
-1	0	1

$$\frac{1}{1298}$$

-19	11	0	-11	19
72	-113	0	113	-72
143	-943	0	943	-143
72	-113	0	113	-72
-19	11	0	-11	19

$$\frac{1}{1038}$$

-10	112	0	-112	10
-27	-166	0	166	27
1	-265	0	265	-1
-27	-166	0	166	27
-10	112	0	-112	10

Filter d   Filter e   Filter f

Fig. 3.   Impulse response of some 2D derivating filters. "d": circulation method, "e" and "f": optimised.
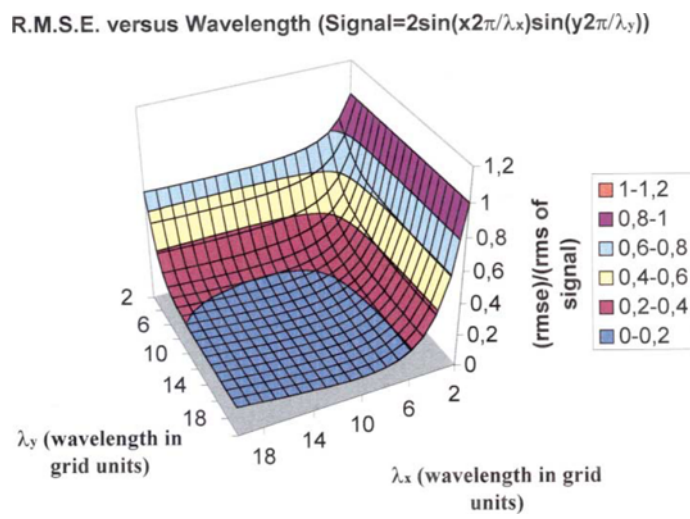
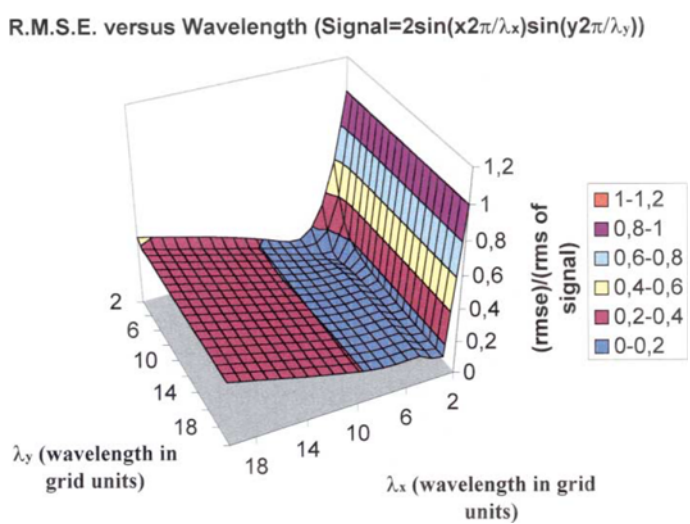Fig. 4.   Total error of 2D derivating filter "d" at different spatial frequencies.

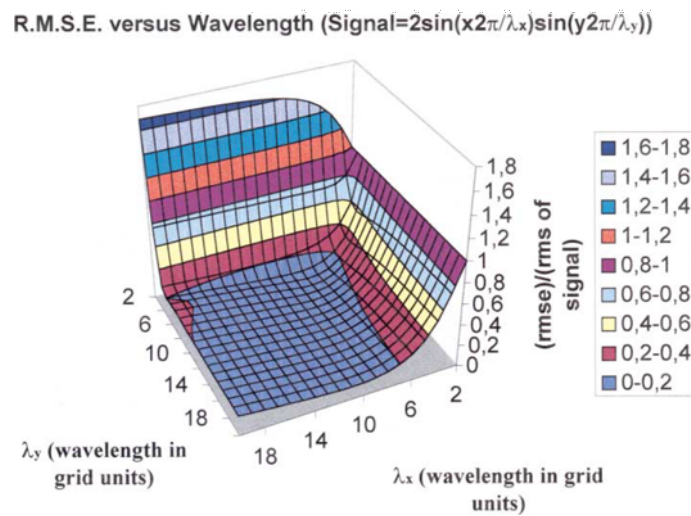Fig. 5.   Total error of 2D derivating filter "e" at different spatial frequencies.

R.M.S.E. versus Wavelength (Signal=2sin(x2π/λx)sin(y2π/λy))

Fig. 6.   Total error of 2D derivating filter "f" at different spatial frequencies.

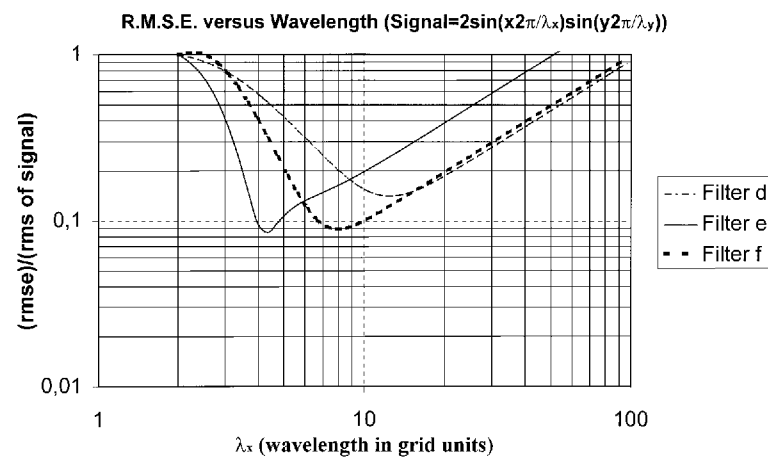**R.M.S.E. versus Wavelength (Signal=2sin(x2π/λx)sin(y2π/λy))**

Fig. 7.   Total error of the 2D derivating filters at different spatial frequencies for the particular case of $\lambda_x = \lambda_y$.

These results show that at long wavelengths an improvement is obtained for the new filters "e" and "f", owing to the built-in extended noise averaging process. At short wavelengths the more non linear variation of the a data along the transverse y axis, owing to the sine function, impairs the accuracy of the 2D filters. The reason for this is that the wavelength of these data is shorter than the filter size.

As a conclusion, the optimized 2D filters can reduce the error over the 1D ones at long wavelengths, but again they can not fulfill the requirement of a wide enough wavelength interval with small error.

3.3. Adaptive Schemes Using 1D Linear Filters

The former two paragraphs induce a conclusion: although so far in this work there has not been found any filter able to give small error over a broad wavelength interval, application of Equation (3) leads to filter optimization on a subinterval that gives, inside it, a very accurate filter. The consequence is obvious, by developing a scheme able to choose the smaller error filter from some formerly developed, depending on the local properties of the data, better results than by using a single one could be achieved. Two of this kind of schemes have been explored:

1. Using a filter optimized for long wavelengths when the output of one optimized for short ones acting on the same data is smaller in magnitude than a certain threshold related to ε. This is because the value of $\Sigma \eta_{i,j}^2 / \alpha$ is

always smaller for filters optimized for long wavelengths. This can be observed in Figs. 7 and 8 and comes from the effect of the second term in Equation (2).

2. It is based on an already documented scheme that detects which one of the two types of error (the ones from the discrete nature of the data or the one from the presence of noise) is larger. This was proposed by Lourenco (1996). From an initial filter, q, two others are developed: w, better at long wavelengths and with similar response at short ones; and e, better at short wavelengths and with similar response at long ones. The way to choose which filter to use at each point is to evaluate the following differences in the response $\mathfrak{R}$: $|\mathfrak{R}w - \mathfrak{R}q| > |\mathfrak{R}e - \mathfrak{R}q| \Rightarrow$ the filter to use is w: $|\mathfrak{R}w - \mathfrak{R}q| < |\mathfrak{R}e - \mathfrak{R}q| \Rightarrow$ the filter to use is e. This scheme fails when the outputs of the similar filters are at both sides of the correct value. An improved version of it, not impaired by this circumstance, is presented below.

It should be remarked that these filter combinations are no longer linear, and response to the sum of components is not equal to the sum of responses. Nevertheless, choosing synthetic flowfields composed by 2D single harmonics seems a reasonable option to initially evaluate the performance of the filters for all the spatial frequencies. This procedure, although not incorporating all the complexities of a real flowfield, seems a very general benchmark. Further investigation using a wide selection of flowfields should confirm this hypothesis.

The use of scheme 1 is simple. Two filters were designed for its implementation. Filter "g": 5 coefficients 1D filter optimized through Equation (3) for short wavelengths, $\lambda_x \in (2.5, 12)$. Filter "h": 5 coefficients 1D filter optimized through Equation (3) for long wavelengths, $\lambda_x \in (8.5, 34)$. Filter "i" results from the scheme application. A threshold level of 3.5 times σ_ε was chosen after extensive testing. In our case this value corresponds to 0.2 times the dynamic range of magnitude a. The suitable threshold level depends mainly on the type and amplitude of noise present in a. The obtained error curve can be observed in Fig. 8, for identical data as before.

- **Filter g:** $\dfrac{1}{1900}$

264	-1478	0	1478	-264

- **Filter h:** $\dfrac{1}{1900}$

-314	-322	0	322	314

- **Filter i:** Uses filter "h" when "g" calculates b with error not higher than the chosen threshold, otherwise it uses filter "g".

R.M.S.E. versus Wavelength (Signal=2sin(x2π/λx)sin(y2π/λy))
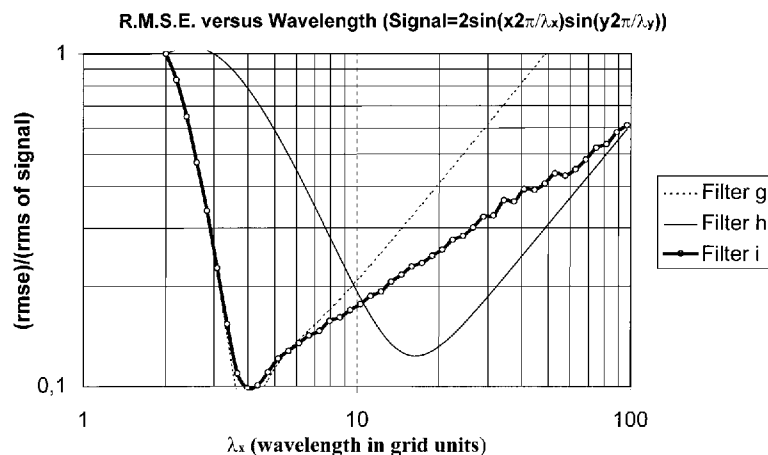
Fig. 8. Total error of the 1D derivating filters "g", "h" and "i" at different spatial frequencies.

Scheme 2 has to be analyzed in detail. The difference between the output of two lineal filters, say "k" and "l", acting on signal a is not uncorrelated but responds to the following equation (through the same considerations that led to Equation(2)):

$$b^k - b^l = \frac{1}{\alpha \Delta x} \sum_{i,j} \left(\left(\eta_{i,j}^k - \eta_{i,j}^l \right) \cdot \left(b^* \sin(i\Delta x) \cos(j\Delta y) + \varepsilon_{i,j} \right) \right) \tag{4}$$

The following nomenclature can be introduced:

$$K_{i,j} = \eta_{i,j}^{k} - \eta_{i,j}^{l} \qquad X_{i,j} = b * \sin(i\Delta x)\cos(j\Delta y) + \varepsilon_{i,j} \tag{5}$$

The just above cited comparison between absolute values of differences between output of two filters ($|\Re w - \Re q| >$ or $< |\Re e - \Re q|$) coincides with checking in the $n+m$ dimensional space of $X_{i,j}$, whether the value of this variable lies between two hyperplanes, defined by its equation coefficients $K_{i,j}^{1} - K_{i,j}^{2}$ and $K_{i,j}^{1} + K_{i,j}^{2}$. Due to the fact that the filters are constrained by the conditions of symmetry and first order accuracy, this scheme works only when the filter has 6 or more non null coefficients. It can be further sophisticated by considering more than two hyperplanes by adding more filters in the choice.

The result of applying these considerations to 1D filters with 9 coefficients gives a reduction of about 15% in the error at some wavelengths, see Fig. 10.

A combination of schemes 1 and 2 was used in filter "l", whose error is shown in Fig. 9.

Two new filters have been designed for an implementation. Filter "j": 9 coefficients 1D filter optimized through Equation (3) for $\lambda_x \in (2.5, 12)$. Filter "k": 9 coefficients 1D filter optimized through equation (3) for $\lambda_x \in (6, 24)$. Filter "l" is the adaptive filter that combines the two schemes. The whole scheme can be reduced to what is indicated as follows:

- **Filter "j":** $\dfrac{1}{1900}$

-9	-57	404	-1551	0	1551	-404	57	9

- **Filter "k":** $\dfrac{1}{1900}$

124	-93	-398	-371	0	371	398	93	-124

- **Filter "l":**Uses filter "k" when either b calculated by filter "j" is lower than 3.5 σ_ε or when all the following filters give an output with the same sign at the point under study. Otherwise it uses filter "j":

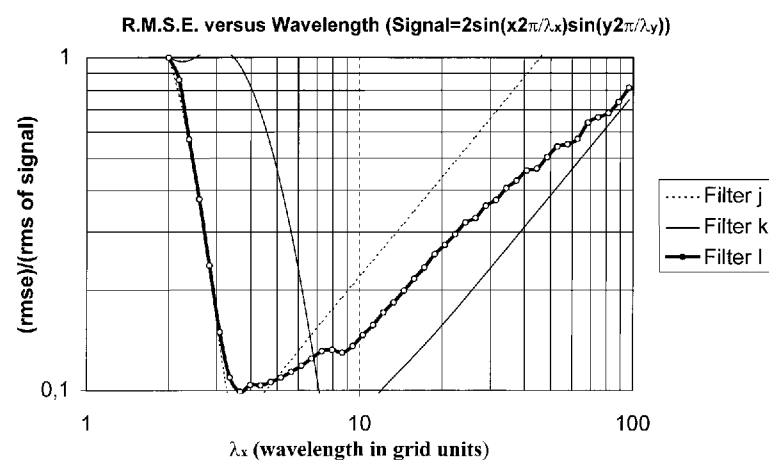| -4	0	1	14	0	-14	-1	0	4
4.5	-7.9	-9	23.7	0	-23.7	9	7.9	-4.5
1	0	-8	12	0	-12	8	0	-1
-1	1	-2	5	0	-5	2	-1	1

Fig. 9.   Total error of 1D "j", "k" and "i" derivating filters at different spatial frequencies.

The advantage of using alone scheme 2 is that there is no need to estimate a threshold. Although it does not show an objectionable error curve, it cannot match the combined scheme. As an example, filter "m" has been obtained, being like filter "l" but without scheme 1. The results are depicted in Fig. 10.
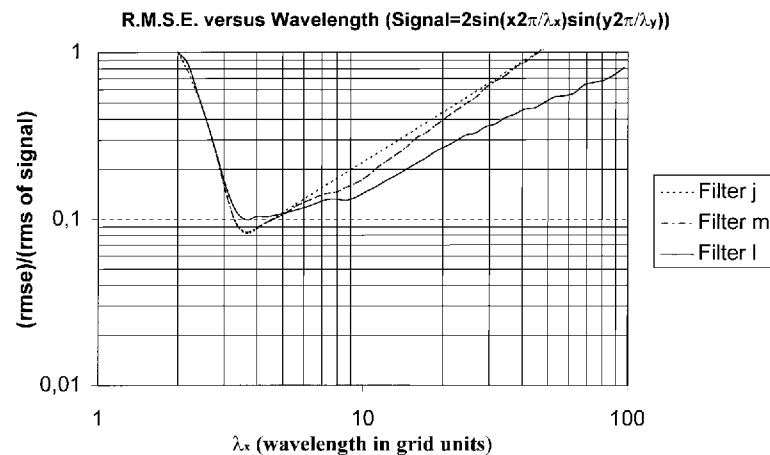
R.M.S.E. versus Wavelength (Signal=2sin(x2π/λ_x)sin(y2π/λ_y))

Fig. 10. Total error of the 1D "j", "m" and "l" derivating filters at different spatial frequencies.

Finally, it should be mentioned that the use of larger filters imply more difficulties on the boundary points: estimation of derived flow magnitudes can not be carried out as close to the border of the image as with smaller ones. One way to deal with this is to design specific filters for the borders. A more practical alternative is to apply usual filters of smaller size to the boundary points, as smaller accuracy is unavoidable in the boundary region.

4. Application to a Typical PIV Output

To offer an indication of the performance of filter "l" on experimentally obtained results, a PIV data set from a reputed laboratory seems suitable. The data corresponds to the flow field shown in Fig. 11. It was obtained from a double exposure PIV image provided by the DLR Göttingen laboratory to the EUROPIV project database. It features the turbulent incompressible flow behind a grid with 28.0 mm mesh size square grid using a rod diameter of 8.0 mm, inside a constant area straight wind tunnel. The free stream is air at 10 m/s and the Reynolds number based on the rod diameter is 5200. The real size of the analyzed flowfield region is 99 mm by 153 mm.

This image was selected for its quality but also for the all over spread of vorticity it shows. The image has been processed using auto-cross correlation with the DANTEC FLOWMAP software, complemented with in house developed routines. The scale factor of the digitized image is 22.33 pixels/mm. The interrogation window size and the distance between vectors are 64 and 32 pixels respectively. Displacement between correlating interrogation windows correspond to the whole image average velocity truncated to the nearest 4 pixel interval. Valid vectors were 99%. Invalid ones were substituted by the average of the 8 neighbors. The density of vectors with which the vorticity calculation has been performed is double (along each axis) than depicted in Fig. 11. The average velocity was subtracted to present the data.

Figure 12 displays the results from filters "b", "d" and "l". Filter "d" shows a noticeable smoothing of noise but at the same time it acts clearly as a lowpass filter. Filter "b" is more accurate when dealing with high frequencies but entails a lower noise smoothing. Filter "l" shows even a better performance for high frequencies than the former one and also seems to smooth noise adequately, as it is the case. For this image more than half of the data points were "k" filtered for at least one of its derivatives. It should be noticed that, since the exact vorticity field is unknown, no absolute conclusion on performance can be obtained out of this figure.
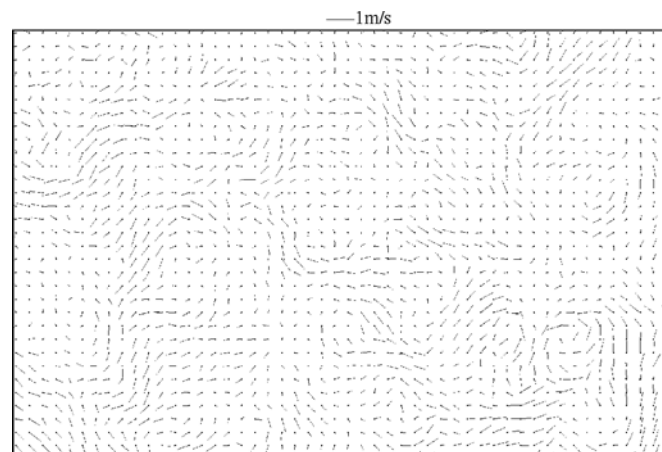
Fig. 11.   Flowfield from real PIV data (from a PIV image provided by DLR Göttingen to the EUROPIV database).

5. Conclusions

An expression to predict the error level of any first derivative linear filter has been developed, under fairly general conditions for the noise content in the data. It has been used to minimize the error on a wavelength interval of the Fourier decomposition of the flowfield. This allowed to show clearly the capabilities and limitations of fixed size linear filters. It allows also to quantify the error of the current filters when applied to any experiment. Although the reality is more complex than here assumed, the proposed formula offers a common simple approach to establish a methodological comparation.

To obtain better derivative filters for the broad wavelengths usually present in a flowfield, adaptive schemes are proposed meaning further refining over the existing ones and even novel ones. As direct application of the work here reported a new adaptive filter is presented and its performance is shown to be advantageous when compared with others already known. The evaluation test includes the vorticity calculation on real PIV data.

An open path is set on the adaptive schemes and also on their use not only for 1D but also for 2D linear filters.
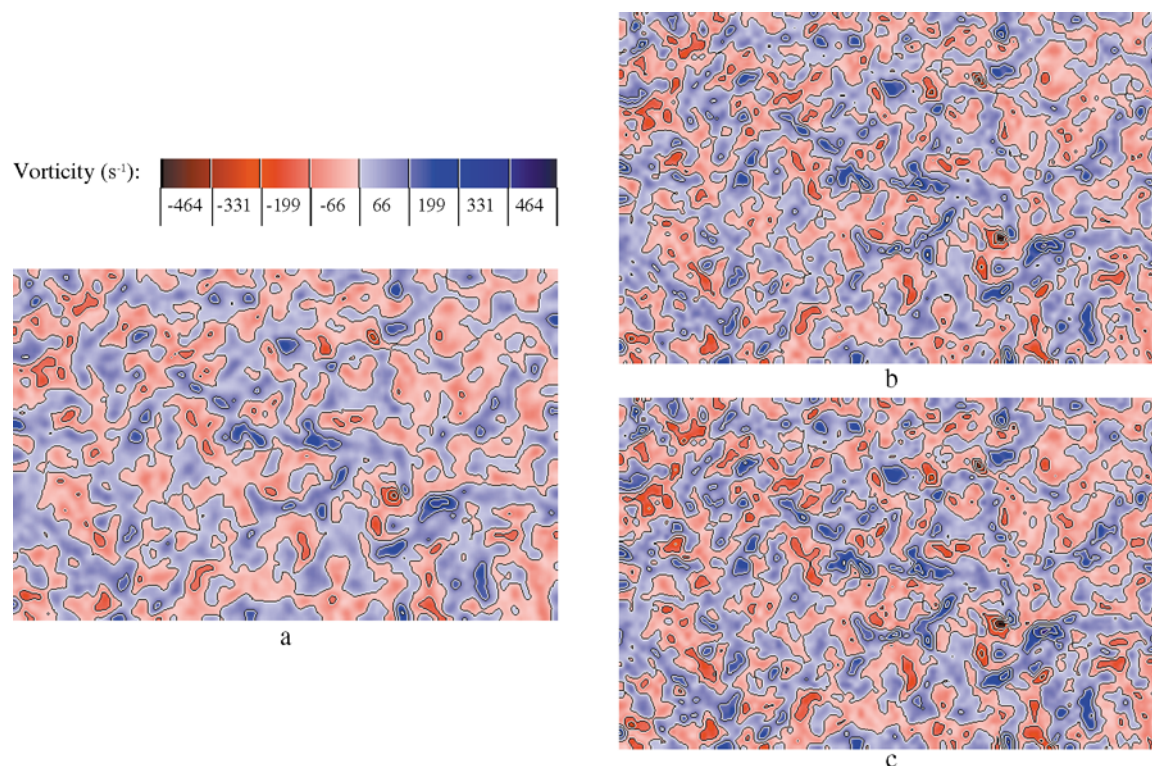

Fig. 12.   Vorticity maps obtained by different first derivative filters for the data depicted in Fig. 11. a) Filter "d"; b) Filter "b"; c) Filter "l".

Acknowledgments

References

Agüí, J. C. and Jiménez, J., On the Performance of Particle Tracking, Journal of Fluid Mechanics, Vol. 185 (1987), 447-468.

Abrahamson, S. and Lonnes, S., Uncertainty in Calculating Vorticity from 2D Velocity Fields using Circulation and Least-squares Approaches, Experiments in Fluids, 20 (1995), 10-20

Lourenco, L. M., Particle Image Velocimetry Post-processing Techniques, Von Karman Institute for Fluid Dynamics Lecture Series, (1996)-03, 88-92

Nogueira, J. I., Lecuona, A. and Rodríguez, P. A., Data Validation, False Vectors Correction and Derived Magnitudes Calculation on PIV Data, Measurement Science and Technology, 8 (1997), 1493-1501.

Raffel, M. and Kompenhans, Post Processing: Data Validation, Von Karman Institute for Fluid Dynamics Lecture Series, (1996)-03.

Authors' Profiles

Pedro A. Rodríguez: He received his degree in Aeronautical Engineering in 1981 from the Universidad Politécnica de Madrid, and his Ph.D. in Aeronautical Engineering in 1985 from the same university, where he worked as Professor in Internal Combustion Engines with Professors Varela and Lecuona. From 1996 he is Full Professor in the Department of Mechanical Engineering at the Universidad Carlos III de Madrid. His research interest focuses on experimental Thermofluidmechanics, with special interest in combustion processes.

Antonio Lecuona: He received his degree in Aeronautical Engineering in 1975 from the Universidad Politécnica de Madrid, and his Ph.D. in Aeronautical Engineering in 1980 from the same university, directed by Professor Amable Liñán. There he worked as Professor in Internal Combustion Engines with Professor Varela. From 1993 he is Full Professor in the Department of Mechanical Engineering at the Universidad Carlos III de Madrid, where he's been appointed also as vicechancellor. His research interest focuses on experimental Thermofluidmechanics, with special interest in combustion processes and Environmental Engineering.

José Ignacio Nogueira: He received his degree in Aeronautical Engineering in 1994 from the Politechnical University of Madrid, and his Ph.D. in Aeronautical Engineering in 1997 from the same university. He worked in the Spanish Air Force before starting his Ph.D. During his Ph.D. he worked as Associate Professor in the Fluid Mechanics and Thermodynamics areas at Carlos III University, with Professors Antonio Lecuona and Pedro Rodríguez. His current position is Visitor Professor in the Department of Mechanical Engineering at Carlos III University. His research interest focuses on experimental Thermofluidmechanics, paying special attention to the Particle Image Velocimetry techniques.